A. Proposal Summary

The relationship between coronal mass ejections (CMEs) and filament eruptions, in the context of their magnetic structure and evolution, has been a fundamental problem in solar physics. However, a number of previous studies including ours have been inconclusive. The major difficulty is that the CMEs is most visible as limb events, while filament eruption and magnetic topology evolution can be best studied when a source region is on the solar disk. The unprecedented data from Earth Connection Coronal and Heliospheric Investigation (SECCHI) on board STEREO provides an unique opportunity to attack this problem, as CMEs and associated eruptions will be viewed at different angles from earth-based observatories. Therefore, both limb CME dynamics and disk signature can be studied simultaneously. We propose to carry out four related tasks.

(1) We will study filament eruptions to be observed by our Global High Resolution Halpha Network and study their response as observed by white-light coronagraphs and EUV Imager(EUVI) of SECCHI. We will construct eruption trajectories from chromosphere through corona to understand the acceleration of filaments and CMEs. Furthermore, we will determine the physical differences between eruptions associated with CMEs and those that are not associated.

(2) We will calculate one of the two components of helicity injection: helicity transport into the solar atmosphere by photospheric footpoint motions (shuffling term). We will study the evolution of helicity injection and compare with the timing of the onset of filament eruptions and CMEs, and correlate the amount of helicity injection with CME kinetics.

(3) We will explore the correlation between the kinetic properties of CMEs and the accompanying magnetic reconnection rate, i.e, the rate of magnetic flux change involved in magnetic reconnection in the low corona. The magnetic reconnection rate is deduced by measuring the expansion of flare ribbons across the magnetic field. We anticipate that this research will provide a clear evidence of the important role of magnetic reconnection in driving large scale eruptions that travel through the interplanetary space. This study with the aided by our newly developed program to automatically detect and track flare ribbons and CME fronts.

(4) Magnetic Clouds

B. Introduction and Objectives of Proposed Research

Filament eruptions, flares, and CMEs are the most important solar events as far as space weather effects are concerned linking solar eruptions, major interplanetary disturbances and geomagnetic storms (Gosling et al., 1991). An earth-directed CME, which is usually associated with activity near solar disk center, has great influence on space weather because of the likelihood to launch geoeffective disturbances toward Earth (Cane et al., 2000; Webb et al., 2000). The sign of magnetic helicity in active regions can be used to predict the orientation of the magnetic field associated with a CME and furthermore, the probability of a geomagnetic storm (Yurchyshyn et al., 2000).

In order to gain a better understanding of CMEs and to improve the reliability of geomagnetic storm predictions and warnings, it is essential to observe early manifestations of CMEs in the solar atmosphere. Thus, our goal is to find possible relationships between solar surface phenomena such as filament eruptions and flares, the CMEs occurrence, and the properties of the associated magnetic field. Once a relationship is found, it can serve as an indicator for the occurrence of geomagnetic storms.

Filaments and prominences refer to the same physical structures on the Sun, either projected onto the disk or extending above the limb. The majority of previous studies have focused on prominences because they could easily be detected, observed, and measured against the dark sky background. Moreover, CMEs, associated with the prominences, are not difficult to detect. Many prominence classifications have been proposed in the past. For example, Gilbert et al. (2000) developed definitions of active prominences (APs) and eruptive prominences (EPs) and studied the relationship between APs, EPs, and CMEs for 54 events. They found that 94% of the EPs had an associated CME compared to only 46% for APs. Gopalswamy et al. (2003) defined a prominence as a radial or a transverse event. Authors showed that the radial events have a strong correlation to the CMEs: 83% of the radial events were associated with CMEs compared to 24% for transverse events. However, Yang and Wang (2002) showed that the connection between filament eruptions observed in Hα and CMEs is weak ranging from 10% to 30%, depending on heliographic location of the source regions (see Figure 1). Based on similar data base, but with larger filament threshold, the percentage of filament eruption associated with CMEs is increase drastically (Jing et al., 2004).

Filament disappearance does not always imply filament eruptions. Depending on their physical nature, disappearing filaments can reappear. Two processes have been proposed by (Mouradian et al., 1995): dynamic sudden disappearance (DSD) and thermal disappearance (THD). DSD is due to restructuring of the magnetic field and it ultimately leads to the disappearance of the filament, whereas THD is due to heating of the plasma in the filament, which will reappear once it cools down. Since THD is not related to magnetic field reorganization, we excluded it from this study.

Based on our successful experience in making high resolution full disk Hα observations at BBSO, and the urgent need to monitor the evolution of the solar chromosphere continuously, we are operating a network for Hα full-disk observations utilizing existing facilities at BBSO in California, the Kanzelhohe Solar Observatory (KSO) in Austria, Catania Astrophysical Observatory (CAO), Yunnan Observatory (YO), and Huairou Solar Observing Station (HSOS) in China. All these observatories have over 200 sunny days a year, good seeing conditions, a sufficient and experienced observing and research staff and well-established Hα telescope systems. Each observatory is now equipped with a 2K$\times$2K digital camera (except CAO which uses 1K by 1K camera). The nominal cadence is 1 minute with 1 arcsecond pixel resolution.

The study of CMEs and filament eruptions in the context of magnetic structure and evolution is important to understand the triggering mechanisms of CMEs. However, a number of studies including ours have been inconclusive. The major difficulty is that the CMEs is most visible as limb events, while filament eruption and magnetic topology evolution can be best studied when a source region is on the disk. The unprecedented data from Earth Connection Coronal and Heliospheric Investigation instrument (SECCHI) on board STEREO provide unique opportunity to revisit this problem, as CMEs and associated eruptions will be viewed at different angles from earth-based observatories. Therefore, both CME dynamics and disk

signature can be studied simultaneously. Coordinated observation provide unique opportunity to reveal 3-D magnetic structure of eruptive events from filament eruption to CME. Our proposed research will be targeted at the following areas:

(1) We will study filament eruptions to be observed by our Global High Resolution Halpha Network and study their response as observed by white-light coronagraphs and EUV imager of SECCHI. We will construct eruption trajectories from chromosphere through corona to understand the acceleration of filaments and CMEs. Furthermore, we will determine the physical differences between eruptions associated with CMEs and those that are not associated.

(2) We will calculate one of the two components of helicity injection: helicity transport into the solar atmosphere by photospheric footpoint motions (shuffling term). We will study the evolution of helicity injection and compare with the timing of the onset of filament eruptions and CMEs, and correlate the amount of helicity injection with CME kinetics.

(3) We will explore the correlation between the kinetic properties of CMEs and the accompanying magnetic reconnection rate, i.e, the rate of magnetic flux change involved in magnetic reconnection in the low corona. The magnetic reconnection rate is deduced by measuring the expansion of flare ribbons across the magnetic field. We anticipate that this research will provide a clear evidence of the important role of magnetic reconnection in driving large scale eruptions that travel through the interplanetary space. This study with the aided by our newly developed program to automatically detect and track flare ribbons and CME fronts.

(4) Magnetic Clouds

C. Research Plan

C.1. Relationship Between Filament Disappearances and CMEs

As we mentioned in the introduction, Yang and Wang (2002) studied about 500 filament disappearances observed in Hα at BBSO and compared them with the corresponding LASCO data. Figure 1 shows the number of filament disappearances as a function of the distance to the solar disk center. The normalized distance mean the physical distance to the solar disk center divided by the solar radius. The lighter histogram is the total number of events, and the darker histogram is the number of the events for which we can find associated CMEs from the LASCO data. We also marked the percentage of events having an associated CME. Please note that this study is different from other studies, such as Gopalswamy et al. (2003) who studied limb events only; and Jing et al. (2004), who selected larger events.

One of the notable examples is the October 13, 1999 event, which is shown in Figures 2 and 3. Figure 2 shows sequence of BBSO full-disk Hα images from October 11 to 15, 1999. The filament eruption occurred at 07UT on October 13. Two magnified images are included to demonstrate the high quality of the full disk data. Figure 3 shows the corresponding CME. This event clearly fits the classical CME picture with a bright rim-like arcade structure, a cavity, plus a core of filament material (Hundhausen, 1988).

The STEREO was successfully launched in October, 2006. It consists of two space-based observatories - one ahead of Earth in its orbit, the other trailing behind. Each is separating from earth at a rate of 22 degrees/year. With this new pair of viewpoints, we will be able to see the structure and evolution of solar eruptions. Sun Earth Connection Coronal and Heliospheric Investigation (SECCHI) is a key instrument on board STEREO. It has four instruments: an extreme ultraviolet imager (EUVI), two white-light coronagraphs and a heliospheric imager. The first three are relevant to our study. These instruments will study the 3-D evolution of CME's from birth at the Sun's surface through the corona and interplanetary medium to its eventual impact at Earth (Howard et al., 2006).

To tract and compare filament eruptions and CMEs, we will combine ground-based full-disk Halpha data with the SECCHI coronograph and EUVI data. Naturally, our five station Global Hα Network will

provide continuous coverage with a cadence of one minute and pixel resolution of one arcsecond. Roughly 1,500 to 2,000 images are obtained each day. At the end of each observing day, a quick video replay of the observations is reviewed by one of the observers in each station, and any notable filament activity is recorded.

When a filament eruption is detected, several new movies from the original 2K$\times$2K digital data will be made to optimize the field-of-view of the targets of observation. The contrast of the filaments/prominences will be enhanced. For example, high resolution movies are made by using partial frames that cover particularly interesting filaments; and prominence movies are made by image enhancement techniques developed at BBSO. These movies will be posted on the BBSO home page promptly. Properties of each erupted filament will be studied in detail, as described below. Excellent time cadence will allow us to distinguish filament eruptions (usually associated with mass motions) from evolutionary changes that may cause a filament to disappear without erupting. As 3-D observations has not been achieved yet due to spacecrafts positions, in Figure 4, we present a CME observed by SECCHI on December 9, 2006 and a full disk Hα image two days later to simulate the situation when a CME is on the limb and the source region is located on the disk from earth-based or earth-aligned observatories.

Most previous studies of the association of activity with CMEs were done in a traditional way – first, identify the onset of CMEs, and then locate optical and other observations to see if there is an associated solar activity (St. Cyr and Webb, 1991; Sheeley et al., 1975; Munro et al., 1979; Webb and Hundhausen, 1987). However, there are two major shortcomings in this approach: (1) CME may be associated with disk counterparts hidden behind the solar limb; (2) Some weak disk CMEs may be overlooked, if one is not assiduously looking for them. We will study this type of association from a different perspective. We will start from Hα movies, catalog every sudden disappearance of prominence and filament, and compare it with the corresponding SECCHI movie to establish the filament eruption/CME association.

There are two most important components in this study.

(1) We determine the physical reason behind the association between filament eruptions and CMEs. It is essential that we obtain a large number of events to study the properties of the two kinds of filament eruptions (here we have already excluded events due to thermal heating); those associated with CMEs, and those not associated with CMEs. Based on comprehensive data comparisons, we will answer the following questions for each of the events:

Does the filament have a sigmoid configuration?

Is it an AR filament or quiet sun filament?

Is it accompanied by a two ribbon flare? Based on the limited samples studied so far, a filament eruption with two ribbon flare is almost always associated with a CME.

Is its size above or a certain threshold? This threshold will be established during our statistic study.

Is it a polar-crown filament?

Is there new flux emergence nearby erupting filaments?

Did the filament reform within certain time scale?

Based on the answers to the above questions, we will find, statistically, if the properties are different for eruptions with and without associated CMEs. If we can find important factors for which a filament eruption is associated with a CME, we may make predictions of CMEs based on the morphology of filaments that are likely to erupt.

(2) We will follow the evolution of filament and CME height to understand the acceleration of eruption process. Again, this is improved with 3-D observations. In Figure 5, we demonstrated an example of our previous study of September 12, 2000 event, where we combine Hα, LASCO and EIT data. For the filament eruptions, we had to assume that it moved in the direction normal to the local surface. Combining SECCHI EUVI and Hα observations will allow accurate determination of eruption direction. This will provide an unique tool to test eruption models starting from chromosphere to corona.

C.2. Helicity Injection Associated with Filament Eruptions

There have been many reports on the helical structure of solar and heliospheric magnetic fields as observed in photospheric magnetic fields (Pevtsov and Canfield, 2000), coronal X-ray images (Canfield and Pevtsov, 1999), solar filaments (Chae, 2001), coronal mass ejections (Rust, 1999), and interplanetary magnetic clouds (Burlaga, 1988). So far most observational studies of the helicity of solar active regions have focused on the current helicity, defined as $\int \mathrm{B}\cdot\mathrm{J}\,\mathrm{dV}$, and its sign (or the linear force-free coefficient α), mainly because they can be directly inferred from photospheric vector magnetograms (e.g., Hagyard and Pevtsov, 1999). The current helicity is a measure of the topological properties, such as twist and mutual linkages of the lines of electric current (Berger and Field, 1984, Devore, 2000). On the other hand, magnetic helicity, defined as $\int \mathrm{A}\cdot\mathrm{B}\,\mathrm{dV}$, is a measure of twist and linkage of magnetic field lines (Devore, 2000). The magnetic helicity is a physically more useful concept than the current helicity, because magnetic helicity is fairly well-conserved in a closed volume, in the absence of boundary flows. It is considered as a robust invariant in space plasmas, such as the solar corona (Berger, 1999). However, this quantity has rarely been measured because of the difficulty in determining the topological connection of field lines in a 3D space. Instead, there have been efforts to determine its rate of temporal change in an open volume.

Since the solar corona is an open volume with the photosphere as a boundary with normal flux, the magnetic helicity can be transported across the boundary by velocity fields in the photosphere. According to Berger and Field (1984), the Poynting theorem for magnetic helicity in an open volume is given by:

$$\frac{dH}{dt} = 2\oint(\mathbf{B}\cdot\mathbf{A}_\mathrm{p})v_z\,dS - 2\oint(\mathbf{v}\cdot\mathbf{A}_\mathrm{p})B_z\,dS \tag{1}$$

where $\mathbf{A}_\mathrm{p}$ is the unique vector potential of the potential field determined by the following conditions:

$$\nabla\times\mathbf{A}_\mathrm{p}\cdot\mathbf{z} = B_z,\ \nabla\cdot\mathbf{A}_\mathrm{p} = 0,\ \mathbf{A}_\mathrm{p}\cdot\mathbf{z} = 0 \tag{2}$$

Equation (1) tells that the magnetic helicity in an open volume can change either by the passage of field lines through the surface (first term) or by the horizontal motions of field lines (second term). The second term is particularly dominant if emerging (or submerging) fluxes are insignificant. The second term is called the shuffling term and the first is the advection term.

The BBSO group has recently studied the injection of helicity into active regions and its possible correlation with the onset of flares. Chae (2001) has developed a tool to derive the second term in the equation from the study of line of sight magnetograms. These are written in equations (3) and (4):

$$A_{p,x} = FT^{-1}[\frac{jk_y}{(k_x^2+k_y^2)}FT(B_z)] \tag{3}$$

and

$$A_{p,y} = FT^{-1}[-\frac{jk_x}{(k_x^2+k_y^2)}FT(B_z)] \tag{4}$$

Chae et al. (2001) studied formation of a filament, and found that the motion of footpoints provide sufficient shuffling helicity into the forming filament. Moon et al. (2002) applied the method to MDI data to study the helicity injection rate associated with several flares, and found a nice correlation between flare energy and amount of helicity injection.

More recently, we studied the relationship between flares and helicity injection (Park et al., 2007). Figure 6 shows the time evolution of the integrated magnetic helicity injection together with total average magnetic flux of the four active regions. The times of X-class flares are presented by the over-plotted GOES soft X-ray light curve. These samples clearly show the helicity variations in two distinct phases: in phase I (starts half to a few days before the flare onset), the helicity accumulates at a nearly constant rate; in phase II (usually

starts 1 to 17 hours before the flare onset and lasts until 1-17 hours after flare), the helicity injection rate is negligible and the magnitude of helicity remains almost constant. In all cases, we can also see a period before phase I, i.e. when the magnitude of helicity remains almost constant without helicity injection. In addition, the positive correlation between the amplitude of the flare and helicity injection rate was found.

We propose to adopt these techniques to extend the study to the evolution of helicity injection rate before, during and after filament eruptions and CMEs. We will select 10 to 20 events, which will satisfy the following criteria:

(1) Regions are close to disk center to avoid confusion arising from geometric projection.

(2) No major observed flux emergence or cancelations, so the advection term can be ignored.

(3) Filament eruptions are associated with CMEs, so that there is substantial amount of energy and mass release, as well as possible helicity transport into interplanetary space. The knowledge we gain here will also help us to understand the physical picture of helicity injection for CMEs.

We will use Hα full disk data to identify the time and location of eruptive events and MDI magnetograms to derive the shuffling term of helicity as described above, and demonstrated in Figures 6. Based on the studies of candidate events, we will learn if the shuffling helicity injection plays an important role in the triggering of filament eruptions. Furthermore, we will convert helicity to the injection of energy, and compare to the energy of associated CMEs. For each event, we will construct helicity injection maps as a function of time, starting two days before an events until two days after, with a cadence between half and one hour. We will be able to find if an impulsive helicity injection is important in triggering filament eruption, in the similar way as is being found for flares (Moon et al., 2002; Park et al., 2007).

We understand that we are only considering the shuffling term in the helicity injection. During the process of selecting events for this study, we will evaluate many events to see if the magnetic flux emergence or cancellation is important in the process of filament eruption. So we will have a by-product of this study, i.e. the percentage of filament eruptions associated with flux emergence or cancellation, and their relative importance in contributing to the advection term in helicity injection. This part is difficult as we need to accurately measure vector magnetic fields as well as velocity fields. Kusano et al. (2002) developed a method of measuring helicity injection rates of both terms associated with flares. It requires the vector magnetograms. In the future, HMI on SDO will provide required data.

One point noteworthy is that based on the studies by Moon et al. (2002) and Chae et al. (2001), the differential rotation did not contribute a major part to the injection of helicity. The shear motion around the neutral line is the major source of helicity injection. We will find out if this conclusion is still valid for the studies of helicity injection associated with filament eruptions. When we accumulate large number of events, we will study the correlation between helicity injection rate, total helicity injection and CMEs speed, acceleration.

C.3. The Relationship between the Rate of Magnetic Reconnection and Solar Eruptions

Magnetic reconnection is considered to play an important role in driving the solar eruptions (filament eruptions and CMEs) as well as giving rise to intense heating that accounts for the associated flares (Lin 2001). Numerous theoretical models for solar eruptions and the evolution of the reconnecting current sheet (RCS) have been developed (e.g., Van Tend & Kuperus 1978; Kaastra 1985; Martens & Kuin 1989; Forbes & Priest 1995; Amari et al. 1996; Lin & Forbes 2000; and see Lin 2003 for review). The rate at which the magnetic flux is converted into the diffusion region, in terms of the electric field E_{rec} in the RCS, can be inferred by measuring the flare ribbon expansion speed V_r and the normal component of the magnetic field B_n swept by the flare ribbons: $E_{rec} = V_r B_n$ (Forbes & Priest 1984). More generally, Lin and Forbes (2000) considered the rate of photospheric magnetic flux change φ_{rec} instead of the electric field in the region of newly closed field lines. The flux change rate can be evaluated by the following equation (Lin & Forbes 2000):

$$\varphi_{rec} = \int E_{rec}\, dl = \frac{\partial}{\partial t} \int B_n\, da \quad , \tag{5}$$

where dl is the length along the RCS and da is the newly brightened area swept by the flare ribbons.

E_{rec} and φ_{rec} provide a measure of the reconnection rate inside the current sheet, and the measurement itself is not dependent on specific models. In this manner, we are particularly interested in the observational signatures of two-ribbon flares that are associated with solar eruptions. We can infer the reconnection rate and compare it with the rising motion of flux-ropes (such as erupting filaments or CMEs). Essentially, the reconnection rate and the flux-rope acceleration focus on important features of the flare. Their connection, therefore, provide a stringent test of the scenarios in which the ejection of solar material and magnetic reconnection are physically linked.

As an example, Figure 7 shows snapshot of an M1.0 flare observed at by Hα Network on 2000 September 12 and corresponding MDI magnetogram, with evolution of flare ribbons marked. It also shows temporal correlation between the flare emissions and reconnection rate for the event on 2000 September 12 and the X1.6 flare on 2001 October 19.

We have been using and will continue to use GHN Hα full-disk images as the primary data source to trace the flare ribbon expansion and the filament rising motion. These Hα observations are suitable because of their high-cadence (one or more image frames per minute), high-resolution (approximately 1 arcsec/pixel) and superior detail and contrast (Martin 1989). The CME height-time data is provided by the LASCO web site that has been compiled by the GSFC group ($http://cdaw.gsfc.nasa.gov/CME_{list}/$). The velocity and acceleration of the filaments and CMEs can be derived numerically as the first and second derivative of corresponding height with respect to time. Initially, MDI magnetograms will be used to measure the longitudinal component of the magnetic fields, which approximate the normal component of the magnetic field B_n because only those flares that occur near the disk center will be under our study. Once again, SECCHI will provide more accurate measurements of CMEs kinetics.

From a sample of 13 well observed two-ribbon flares, that are associated with filament eruptions or CMEs, acceleration of erupting filaments is mainly in the range of $0.05-0.4 kms^{-2}$, up to $3 kms^{-2}$. The maximum E_{rec} and φ_{rec} mostly occur in the range of $0.2-5 Vcm^{-1}$ and $0.5-6\times10^{18} Mxs^{-1}$, respectively. In the case of the extremely dramatic flare on October 29, 2003, E_{rec} reaches a magnitude of about $38 Vcm^{-1}$. We found the electric field is generally comparable with most observational results (Poletto & Kopp 1986; Wang et al. 2003, 2004; Qiu et al., 2004) and simulation results (Martens & Kuin 1989; Lin 2002; Cheng et al. 2003). The electric field strength found above implies strong heating and particle acceleration which are responsible for the high energy emissions (Cheng et al. 2003; Qiu et al. 2002, 2004). The left two panels of Figure 8 displays scatter plots of the reconnection rate (namely, E_{rec} and φ_{rec}) versus the acceleration of filaments in a logarithmic scale. All values refer to their maximal that were found on each events. Certain linear correlation between filament acceleration and reconnection rates is demonstrated, but need more events to confirm. Combined SECCHI, Hα and MDI/HMI data will provide unique opportunity for this study.

Due to the temporal-spatial gap between the disk observations of the flares that involve magnetic reconnection and LASCO observations of CME fronts, it is less meaningful to compare the magnetic reconnection rate and the CME acceleration. Instead, we use the velocity of CMEs at C2 to examine the relationship between CMEs and flares in that the velocity is the cumulation of the acceleration at its early stage ($Vel_{CME} = \int Accel_{CME}\, dt$) and, therefore, in some way conveys information about the acceleration during that stage. A graphical display of the CME velocity versus the reconnection rate is presented by two panels on the right side of Figure 8. The figure suggests some weak correlation between them.

More recently, Qiu and Yurchyshyn (2005) explored relationship between the total reconnection flux estimated from flare observations and the velocity CMEs. It is shown that the velocity of CME is proportional to the total reconnection flux, with a linear cross-correlation of 89% and confidence level greater than 99.5%. This result confirms the importance of magnetic flux transferred by magnetic reconnection in the early stage

of fast CMEs. Figure 9 shows their results.

In summary, with the limited sample, we had found certain magnitude scaling relationship between the magnetic reconnection rate and the kinetics of erupting filaments and CMEs. These pilot results need to be certified by including more events to improve the statistical significance. In order to achieve this goal, we will improve our automatic program to align Hα images and MDI magnetograms, count all brightened pixels swept by flare ribbons in a sequence of consecutive Hα images and then map them to the co-registered longitudinal MDI magnetograms. This program, mainly based on "region growing", "adaptive boundary-base" and "morphological closing" methods, makes batch processing possible. Moreover, it is important to determine whether the relationship is independent of the magnetic configurations of source regions and the structure of CMEs. If and when the correlation relationship can be solidly established, we will provide a real-time prediction of filament accelerations and its associated CME speeds, based on the real-time monitoring of flare ribbon separation.

D. Association Between CMEs and MC

It well known now that geomagnetic storms are caused by the southward magnetic field associated with Earth directed CMEs (Burlaga et al., 1981; Wilson & Hildner 1983; Zhang et al., 2003). Interplanetary CMEs (ICMEs) often consist of a shock region with magnetic sheath that preceed ICME body or ejecta. Southwardly directed fields in the sheath region can lead to a rapid storm onset. Very often, however, the sheath's fields rapidly fluctuate, so it can not impose prolonged southward fields and thus its geomagnetic effect is not very strong. An ICME body very often produces persistent high magnitude south fields that have the potential to cause the greatest magnetospheric effects (Rostoker & Fälthammar 1967; Russell et al., 1974; Tsurutani et al., 1992).

Earth-directed CMEs are often seen in coronagraphs as bright expanding halos surrounding the Sun. The corresponding ICME body (or ejecta), is then of ten observed near the Earth as a magnetic cloud (MC, Burlaga et al., 1981, Bothmer and Schwenn, 1998). Generally, MCs exhibit a magnetically organized geometry, which is thought to correspond globally to a curved flux rope (Bothmer and Schwenn, 1998). Estimations of the fraction of ejecta that are MCs vary between 14% and 80%, depending on the criteria used for MC identification. For broader discussion of this problem we refer the reader to a study by Richardson & Cane (2004).

Depending on the orientation of the magnetic field in an ICME (i.e., magnetic flux rope), it may, or may not, impose an intense southward (negative) B_z field. *Therefore, the successful prediction of the structure (orientation, in particular) of CME related magnetic fields in a solar wind is a top-priority in Space Weather studies.*

Current predictions are based on the fact that twist and orientation of the magnetic field in solar filaments outside active regions correspond to those in MCs (Bothmer & Schwenn 1994; Rust 1994; Marubashi 1997; Zhao & Hoeksema 1998; McAllister & Martin 2000; Yurchyshyn et al., 2001, 2005, 2006; Ruzmaikin et al., 2003; Ishibashi & Marubashi 2004; Hu et al., 2005; Gopalswamy et al., 2005; Rust et al., 2005; Krall et al., 2006; Wang et al., 2006). Although some findings are inconclusive (Leamon et al., 2002, 2004; Wang et al., 2006) and there is no well developed scheme to predict the internal structure of an ICME based on solar magnetograms and coronal images.

One of the problems is that LASCO data provide us with the 2D projection of a 3D ejecta, therefore the projection effect van greatly affect the observed shape and the expansion speed of halo CMEs (Zhao et al., 2002; Xie et al., 2004; Zhao 2005; Michalek et al., 2006). Therefore, *a multipoint view of solar active redions and MCs, provided by STEREO, would substantially progress our current understanding of the solar field structure and its relationship to the origin of geoeffective ICMEs.*

CMEs that erupt close to the solar limb and are seen from the side (Figure 1) often exhibit a three-part structure that is commonly interpreted as an expanding magnetic flux rope (Chen et al., 1997, Low,

2001). Cremades & Bothmer (2004) examined 124 CME limb events and concluded that their white-light morphology bears information of the magnetic structure. These authors also argue that the structured CMEs are magnetically organized in the axial direction, which corresponds to the axis of a large-scale twisted flux rope.

Krall et al. (2006) modelled the well-known 2003 October 28 event as an erupting flux rope and generated a synthetic coronagraph image of this model âĂIJhaloâĂİ which appeared to be elongated in the direction of the flux rope axial field, thus indicating that the ellipse-shaped appearance of halo CMEs may be related to their magnetic structure (see Figures 2 and 8 in Krall et al., 2006). This suggestion was further supported in Yurchyshyn et al. (2006).

The findings mentioned above motivated us to study whether there is any correlation between the estimates of orientation angles of MCs and the tilt of elongated CMEs, and to understand if the elongation indicates the axial direction of an underlying flux rope. In the present paper, we describe a statistical comparison of orientations of 25 CME–MC pairs. We note that the halo and MC angles are compared without addressing handedness of the underlying flux rope field.

We have conducted a study (Yurchyshyn et al. 2007 [1]) of 25 CME–MC pairs, which where carefully selected to ensure a realiable correspondence between solar and interplanetary events. The majority of the selected CME-ICME events are those listed in the Master Data Table compiled during the LWS CDAW workshop. We also used some events studied in Qiu & Yurchyshyn (2005).

The CME orientation angles were determined by fitting an ellipse to an irregularly-shaped "halo" around the occulting disk and its tilt angle, α_{CME} was measured in the clockwise direction from the positive *y*-axis of the GSE coordinate system.

For each event in our list we applied a Grad-Shafranov (GS) reconstruction routine (Hu & Sonnerup 2002) to determine the orientation angle of the corresponding MC, α_{GS}. (Note, that some MCs could not be resolved by the GS routine). We also used the orientation angles independently determined with the MC fitting routine (Lepping et al., 1990) by Lynch et al. (2005, herein LY), α_{LY}, and the Wind MFI Team (Lepping et al., 2006, herein MFI), α_{MFI}. The MC orientation angle is measured in the clockwise direction from the positive *y*-axis toward the MC flux rope axis projected onto the GSE *yz* plane. For three events (Oct 28, 2003, Nov 18, 2003 and May 13, 2005) we used orientation angles produced by the erupting flux rope model (see Krall et al. (2006) for details of the MC fitting).

In Figure 10 the major axes of the filled ellipses indicate orientations of the observed CMEs, while various arrows represent results from the GS reconstruction (green), MC fitting by Lynch et al. (2005, black) and Lepping et al. (2006, red solid) and the EFR model (dashed red). For each CME–MC pair we calculated the mean MC orientation angle (black and white (BW) dotted arrow) and those pairs for which the difference between the CME and MC angles is less than 45 deg are shown with long BW dotted arrow inside green boxes and. Events with the difference angle larger then 45 deg are shown with red boxes.

We then calculated the ratio of the CME–MC pairs with a good corresponance (green boxes) to the total number of events and found that *for 64% of CMEs, their elongation indicates the orientation of MC at 1AU.*

We are aware that some partial halos may be of a circular or irregular shape and in this case the apparent CME elongation is due to projection effect and it may have little relationship to the flux rope axis. Thus, according to the CME Catalog, all 7 out of 9 "red events" are halos with "outline assymetry", in other words, they are partial halos or assymetrical halos. Moreover, Zhao (2007[2]) examined 17 halo CMEs by using elliptical cone model and i) successfuly confirmed our findings, while ii) concluding that for some assymetrical events in our data list the projection effect can be substantial and it should be taken into account.

These studies clearly demonstrate that CMEs, observed with coronographs may be the key to solving the long standing problem of magnetic field orientations. Although we seem to understand how and what information can be extracted from the images, the projection effect and the single point view are obstacle

[1] `http://www.bbso.njit.edu/~vayur/VYurchyshyn_etal_COSPAR_2006.pdf`

[2] also at `http://cism.fit.edu/LWS-CDAW_2007_Schedule.html`

to a successful solution. Further studies are needed to understand the obtained correspondence rate as well as to explain the observed differences between the CME and MC angles. STEREO data will provide an unprecedented view of a coronal ejecta from two different point of views. These data, combined with sophisticated techniques of data analysis (such as inversion of the cone model for halo CME, Zhao, 2006), will provide us with accurate information on CME structure and orientation.

By analyzing a combined data set that includes STEREO solar surface data (see prev. sections), LASCO and STERO coronographic images as well as ACE MC measurements we will focus the problem of the relationship between solar eruptive phenomena, coronal mass ejections and the associated interplanetary disturbances. More specifically, the following questions will be addressed:
1) what is the relationship between erupting filaments (Section C.1) and interplanetary fields observed at 1AU in terms of magnetic field orientation and twist?
2) what is the relationship between the reconnection rate (Section C.3), CME speeds and the magnitude of the B_z in MC?
3) what is the correspondence rate between CME elongation and MC orientation?
4) how the accuracy of MC fitting affects the correspondence rate?
5) is there any regular pattern in the rotation of CMEs?
6) if so, can we use this pattern to guide heliospheric modeling and space weather forecast?
7) what is the role of the heliospheric current sheet in the CME deflection, if any?.
$\Rightarrow$ **We realize potential difficulties and uncertainties related to this study.**
I) While the basic suggestion – CME elongation indicates the orientation of the underlying flux rope – seems reasonable, the results, i.e., the correspondence rate, is not very impressive. We see three possible reasons that could contribute to this outcome: 1) MC fits for some events are not reliable; 2) orientation angles for some partial halo CMEs are affected by the projection effect and 3) some CMEs may rotate as they expand. We believe that an comprehensive study based on STEREO data will enable us to untangle those contributions and better understand CME evolution.
II) Solar wind data are one point measurements and MC parameters produced by the state-of-the art models are intrinsically "noisy". Also, MC fitting results are, in general, sensitive to the MC boundaries that are normally chosen by the modeler. This is a typical problem with many MC studies. Improved data such as STEREO CME observations and multi-point solar wind measurements can substantially change the quality and reliability of the fits.

E. Personnel and Budget

This research project will be carried out by the four-member research team: PI Wang, Co-Is Drs. Yurchyshyn, Jing and a Ph.D. student. Dr. Yurchyshyn is a research professor at BBSO Dr. JING is a post-doctoral research fellow at NJIT. Although the entire team will work closely, each individual will focus on particular area. Dr. Jing will be primarily responsible for calculating magnetic reconnection rate, as she has substantial experience in this area. Dr. Yurchyshyn will primarily carry out study on magnetic clouds. Wang will work closely with Mr. Park, a Ph.D. student, to carry out statistical studies of filament eruptions and CMEs, and magnetic helicity. Wang's contribution is completely paid by NJIT.

F. References Cited

Berger, M.A., 1999, Geophys. Monogr. 111, 1

Berger, M.A. and Field, G.B., 1984, J. Fluid Mech., 147, 133

Bothmer, V., Schwenn, R. 1998, Annales Geophysicae, 16, 1

Bothmer, V., & Schwenn, R. 1994, Space Science Reviews, 70, 215

Burlaga, L. F., Sittler, E., Mariani, F., & Schwenn, R., 1981, J. Geophys. Res., 86, 6673

Burlaga, L.F., 1988, JGR, 93, 7217

Cane, H. V., Richardson, I. G. & St. Cyr, O. C., 2000, Geophys. Res. Lett., 27, 3591

Canfield, R.C and Pevtsov, A.A., 1999, Geophys. Monogr. 111, 197

Chae, J., 2001, Ap. J., Letters, 560, L95

Chae, J., Denker, C., Spirock, T. J., Wang, H. and Goode, P., 2000, Solar Physics, 195, 333

Chae, J., Wang, H., Wang, H., Qiu, J., Goode, P. R., Strous, L. and Yun, H. S., 2001, Ap.J., 560, 476

Cheng, C. Z., Ren, Y., Choe, G. S. & Moon, Y. J., 2003, ApJ, 596, 1341

Cremades, H., & Bothmer, V., 2004, Astron. Astrophys., 422, 307

DeVore, C.R., 2000, Ap.J., 539, 944

Forbes, T. G. & Priest, E. R., 1995, ApJ, 446, 377

Hagyard, M. J. and Pevtsov, A. A., 1999, Solar Physics, 189, 25

Gilbert, H. R., Holzer, T.E., Burkepile, J. T. and Hundhausen, A., 2000, Ap.J., 537, 503

Gopalswamy, N., Shimojo, M., Lu, W., Yashiro, S., Shibasaki, K. & Howard, R. A. 2003, ApJ, 586, 562

Gopalswamy, N., Yashiro, S., Michalek, G., Xie, H., Lepping, R. P., & Howard, R. A., 2005, Geophys. Res. Lett., 32, 12

Gosling, J. T., McComas, D. J., Phillips, J. L. & Bame, S. J., 1991, J. Geophys. Res., 96, 7831

Hu, Q., & Sonnerup, B. U. Ö., 2002, J. Geophys. Res., 107, CiteID 1142, DOI 10.1029/2001JA000293

Hu, Q., Smith, C. W., Ness, N. F., & Skoug, R. M. 2005, J. Geophys. Res., 110, 9

Howard et al., 2006, AGU, 12A-02H

Hundhausen, A.J., 1988, Proceedings of 6th International Solar Wind Conference, ed. V.J. Pizzo

Ishibashi, H. & Marubashi, K., 2004, geophys. Res. Lett., 31, 21807

Jing, J., Yurchyshyn, V. B., Yang, G., Xu, Y. & Wang, H., 2004, Ap.J., 614, 1054

Jing, J., Qiu, J., Lin, J., Qu, M., Xu, Y. & Wang, H., 2005, Ap.J., 620, 1085

Kaastra, J. S. 1985, Ph.D. thesis, Univ. Utrecht

Krall, J., Yurchyshyn, V.B., Slinker, S., Skoug, R.M., & Chen, J., 2006, Astrophys. J., 642, 541

Kusano, K., Maeshiro, T, Tokoyama, T. and Sakurai, T., 2002, Ap.J., submitted

Leamon, R. J., Canfield, R. C., & Pevtsov, A. A. 2002, J. Geophys. Res., 107, 1

Leamon, R. J., Canfield, R. C., Jones, S. L., Lambkin, K., Lundberg, B. J., & Pevtsov, A. A. 2004, J. Geophys. Res., 109, 5106

Lepping, R. P., Jones, J. A., & Burlaga, L. F., 1990, J. Geophys. Res., 95, 11957

Lepping, R. P., Berdichevsky, D. B., Wu, C.C., Szabo, A., Narock, T., Mariani, F., Lazarus, A. J., & Quivers, A. J., 2006, Annales Geophysicae, 24, N1, 215

Lin, J., 2001, Ph.D. thesis, Univ. New Hampshire

Lin, J., 2003, NewA Rev., 47, 53

Lin, J. & Forbes, T. G., 2000, J. Geophys. Res., 105, 2375

Lynch, B.J., Gruesbeck, J.R., Zurbuchen, T.H., & Antiochos, S.K., 2005, J. Geophys. Res., 110, A08107

Martens, P. C. H. & Kuin, N. P. M., 1989, Sol. Phys., 122, 263

Martin, S. F. 1998, Sol. Phys., 182, 107

Marubashi, K., 1997, in *Coronal Mass Ejections*, Geophysical Monograph 99, ed. N. Crooker, J.A. Joselyn, & J. Feynman, Washington , DC: AGU, 137

McAllister, H., & Martin, S. F. 2000, Advances in Space Research, 26, 469

Michalek, G., Gopalswamy, N., Lara, A., Yashiro, S., 2006, Space Weather, 4, S1003, 10.1029/2005/SW000218

Moon, Y., Chae, J., Wang, H., Park, Y., Choe, G. and Goode. P.R., 2002, Ap. J., in press

Mouradian, Z, Soru-Escaut, I. and Pojagas, S. 1995, Solar Physics, 158, 269

Munro, R.H., Gosling, J. T., Hildner, MacQueen, R.M., Poland, A. I. and Ross, C.L., 1979, Solar Physics, 61, 201

Park, S. et al., 2007, Ap.J., submitted

Pevtsov, A.A. and Canfield, R.C., 1999, Geophys. Monogr. 111, 93

Poletto, G. & Kopp, R. A., 1986, in The Lower Atmosphere of Solar Flares, ed. D. F. Neidig (Sunspot: NSO), 453

Qiu, J., Lee, J., Gary, D. E. & Wang, H., 2002, ApJ, 565, 1335

Qiu, J., Wang, H., Cheng, C. Z. & Gary, D. E. 2004, ApJ, 604, 900

Qui, J. & Yurchyshyn, V., 2005, Ap.J. Letters, 634, L121

Richardson, I. G., & Cane, H. V., 2004, J. Geophys. Res. , 109, 9104

Rostoker, G. & Fälthammar, C.-G., 1967, J. Geophys. Res., 72, 5853

Russell, C.T., McPherron, R.L., & Burton, R.K., 1974, J. Geophys. Res., 79, 1105

Rust, D. M., 1994, geophys. res. Lett., 21, 241

Rust, D.M., 1999, Geophys. Monogr. 111, 221

Rust, D. M., Anderson, B. J., Andrews, M. D., Acuña, M. H., Russell, C. T., Schuck, P. W., & Mulligan, T. 2005, Astrophys. J., 621, 524

Ruzmaikin, A., Martin, S., & Hu, Q., 2003, J. Geophys. Res., 108, 13

Sheeley, N.R. Jr and twelve others, 1975, Solar Physics, 45, 377

Stcyr, O. C. and Webb, D.F., 1991, Solar Physics, 136, 379

Tsurutani, B.T., Lee, Y.T., Gonzalez, W.D., & Tang, F., 1992, Geophys. Res. Lett., 19, 73

Van Tend, W. & Kuperus, M., 1978, Sol. Phys., 59, 115

Wang, H., Qiu, J., Jing, J. & Zhang, H., 2003, ApJ, 593, 564

Wang, Y., Zhou, G., Ye, P., Wang, S., Wang, Y., 2006, Astrophys. J., 651, 1245

Webb, D.F., and Hundhausen, A. J., 1987, Solar Physics, 108, 383

Webb, D. F., Cliver, E. W., Crooker, N. U., St. Cyr, O. C. & Thompson, B. J., 2000, J. Geophys. Res., 105, 7491

Wilson, R.M., & Hildner, E., 1984, Solar Phys., 91, 169

Xie, H., Ofman, L., & Lawrence, G., 2004, J. Geophys. Res., 109, 3109

Yang, G. & Wang, H., 2002, in COSPAR Colloq. Ser. 14, Solar-Terrestrial Magnetic Activity and Space Environment, ed. H. Wang & R. Xu (Boston: Pergamon), 113

Yurchyshyn, V. B., Wang, H., Goode, P. R. & Deng, Y., 2001, ApJ, 563, 381

Yurchyshyn, V., Hu, Q., & Abramenko, V., 2005, Space Weather, 3, No. 8, S08C02

Yurchyshyn, V., Liu, C., Abramenko, V., & Krall, J., 2006, Solar Phys., 239, 317

Yurchyshyn, v., Q. Hu, R.P. Lepping, B.J. Lynch & J. Krall, 2006, Adv. Space Res., (http://dx.doi.org/10.1016/j.asr.2007.01.

Zhang, J., Dere, K.P., Howard, R.A., & Bothmer, V., 2003, Astrophys. J., 582, 520

Zhao, X. P., & Hoeksema, J. T., 1998, J. Geophys. Res., 103, 2077

Zhao, X.P., Plunkett, S.P., & Liu, W., 2002, J. Geophys. Res., 107, 13

Zhao, X.P., 2005, IAU Symp. 226, *Solar and Stellar mass Ejections*, ed. Dere, K., & Wang, J., & Y. Yan, Cambridge: Cambridge University Press, 42

Zhao, X. P., 2006 AGU Fall Meeting, abstract #SH43B-1521

Zhao, X.P., 2007, private communication, also in preparation

Figure 1: Distribution of filament disappearance as function of the distance from the disk center. The lighter histogram is the total number of events, and the darker histogram is the number of events with associated CMEs found from the LASCO data. We also indicated at the top of each bar the percentage of events for which LASCO events have been identified.

Figure 2: The sequence of Hα full-disk images demonstrating the disappearance of a major filament inside the white box. A Kitt Peak magnetogram at 15:43 on October 13 is also included to show the magnetic configuration. In the second row, we show a magnified field of view from the same images in the first row to demonstrate that the fine structure can be resolved by our full disk images.

Figure 3: The LASCO C2 image shows the CME corresponding to the filament disappearance in Figure 2.

Figure 4: Comparison of a CME observed on December 9, 2006 as observed by COR2/SECCHI on board STEREO (left) and a full disk Halpha obtained at BBSO on December 11, 2006. This simulates the situation when the STEREO has a view angle of about 60 degrees away from earth's observations. Then the center region active region's CME will be view clearly as limb event.

Figure 5: Left panel: time profiles of the flare ribbon separation, filament heights measured from KSO and EIT images, and CME heights measured by Dr. Yashiro ($http://cdaw.gsfc.nasa.gov/CME\_list/$). The lines indicate the least-squares fits to hyperbolic functions. Right: velocity profiles of the ribbon separation, filament, and CME derived from the fits of the height profiles.

Figure 6: Time profiles of helicity injection, magnetic flux and GOES X-ray flux for 4 active regions. The helicity is shown as crosses; the dotted lines are the GOES X-ray flux and total average magnetic flux are shown as diamonds. The flux is averaged of the absolute sum of positive and negative fluxes.

Figure 8: Top-left: Scatter plot of maximum filament acceleration vs. maximum φ_{rec}; Bottom-left: Scatter plot of maximum filament acceleration vs. maximum E_{rec}. Top-right: Scatter plot of CME velocity at C2 vs. maximum φ_{rec}; Bottom-right: Scatter plot of CME velocity vs. maximum E_{rec}. Error bars attached to each sign indicate the uncertainty of the measurement (Jing et al., 2005).

Figure 9: Scatter plot of CME velocities vs. total reconnection flux for 13 events. Dark and gray colors indicate events associated with erupting and non-erupting filaments, respectively. The dashed guideline shows the least-squares linear fit to the data points (Qiu and Yurchyshyn, 2005).

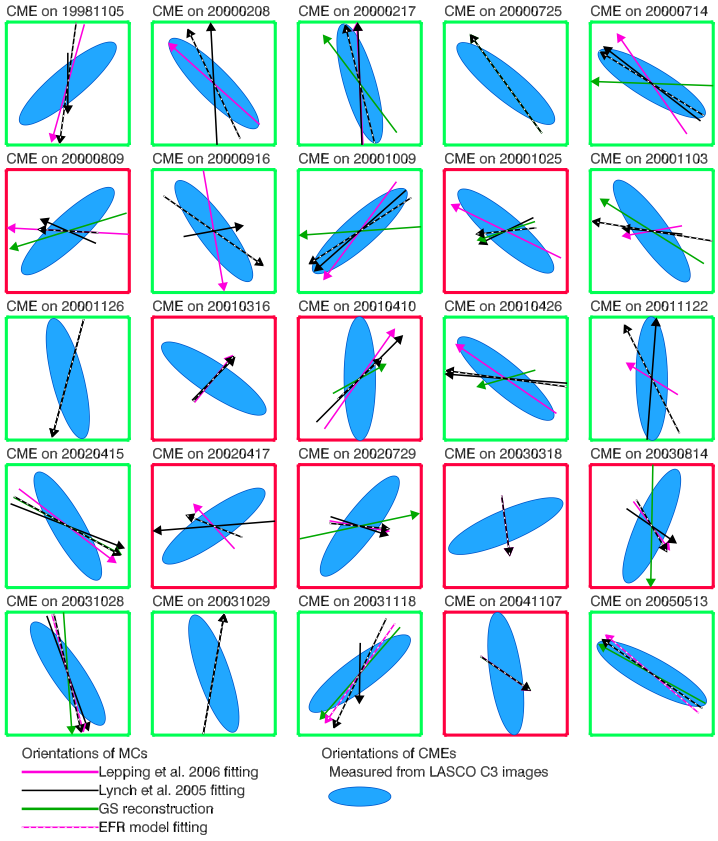

Figure 10: Comparison between the LASCO CME (filled ellipses) and MC clock angles. Long (short) arrows indicate cases when the difference between the LASCO and MC clock angles is smaller (exceeds) than the threshold of 45 deg.